http://dx.doi.org/10.5012/bkcs.2013.34.7.2067

Effect of Hydrogen Treatment on Anatase TiO_2 Nanotube Arrays for Photoelectrochemical Water Splitting

Hyun Sik Kim and Soon Hyung Kang[†,*]

School of Chemical & Biological Engineering, Seoul National University, Seoul 151-742, Korea
[†]Department of Chemistry Education, Chonnam National University, Gwangju 500-757, Korea. [*]E-mail: skang@jnu.ac.kr
Received January 22, 2013, Accepted April 13, 2013

Hydrogen (H_2) treatment using a two-step TiO_2 nanotube (TONT) film was performed under various annealing temperatures from 350 ºC to 550 ºC and significantly influenced the extent of hydrogen treatment in the film. Compared with pure TONT films, the hydrogen-treated TONT (H:TONT) film showed substantial improvement of material features from structural, optical and electronic aspects. In particular, the extent of enhancement was remarkable with increasing annealing temperature. Light absorption by the H:TONT film extended toward the visible region, which was attributable to the formation of sub-band-gap states between the conduction and valence bands, resulting from oxygen vacancies due to the H_2 treatment. This increased donor concentration about 1.5 times higher and improved electrical conductivity of the TONT films. Based on these analyses and results, photoelectrochemical (PEC) performance was evaluated and showed that the H:TONT film prepared at 550 ºC exhibited optimal PEC performance. Approximately twice higher photocurrent density of 0.967 mA/cm^2 at 0.32 V *vs.* NHE was achieved for the H:TONT film (550 ºC) *versus* 0.43 mA/cm^2 for the pure TONT film. Moreover, the solar-to-hydrogen efficiency (STH, η) of the H:TONT film was 0.95%, whereas a 0.52% STH efficiency was acquired for the TONT film. These results demonstrate that hydrogen treatment of TONT film is a simple and effective tool to enhance PEC performance with modifying the properties of the original material.

Key Words : Hydrogen treatment, TiO_2 nanotube, Doping effect, Photoelectrochemical water splitting

Introduction

Photoelectrochemical (PEC) water splitting to produce solar hydrogen has been an increasingly interesting field since Honda and Fujishima's demonstration of water photo-oxidation on a *n*-TiO_2 photoanode in 1972.[1] PEC converts water into hydrogen and oxygen as an attractive form of artificial photosynthesis. Considerable efforts have been devoted to develop suitable photoanode materials and new nanostructure design to overcome the reported solar-to-hydrogen conversion (STH) efficiency compared with the theoretically expected value.[2-6] Among a variety of photoanode materials such as the cheap metal oxides, TiO_2, WO_3, α-Fe_2O_3, and $BiVO_4$, TiO_2 is a well-known candidate for water photo-oxidation and has been widely studied because it is highly resistant to photocorrosion, nontoxic, abundant, and has strong photocatalytic efficiency.[6,7] However, the STH efficiency of TiO_2 remains $< 2.2\%$ under sunlight conditions due to its large band gap (3.0-3.2 eV), limited absorption of sunlight in the visible region, low electron mobility (1 cm^2/V·s), and short minority carrier (hole) diffusion length (10-100 nm).[8] Accordingly, one-dimensional (1-D) nanostructures such as nanowires, nanotubes, and nanorods are advantageous over planar geometries because these structures permit considerable light absorption depths, enhanced charge separation by providing high electrode/electrolyte interface areas, and a reduction in the charge carrier transport distance to the electrolyte, which increases quantum efficiency.[9]

In addition, some dopants such as nitrogen (N), carbon (C), and hydrogen (H) serve as electron donors to contribute to light absorption in the visible region and increase the electrical conductivity of the film.[10] In particular, the valence band edge of nonmetal (N, C)-incorporated TiO_2 is upshifted by forming impurity states above the valence band or hybridizing with O 2*p* states to extend the absorption spectrum toward the visible light region.[11] In contrast, H:TiO_2 creates oxygen vacancy sites; thus, forming donor states below the conduction band, which improves charge transport and light absorption similar to *n*-type doping, thereby enhancing PEC performance.[12] Therefore, hydrogen treatment based on a 1-D nanostructure photoanode can offer a synergetic effect with modifications of the intrinsic electrical properties of a TiO_2 material as well as the strong points of 1-D nanostructures. 1-D nanotubes were thermally treated in an H_2 atmosphere at various temperatures to demonstrate the decoupling effects in TiO_2, which substantially increased donor density and was closely correlated with electrical conductivity and charge transportation. Therefore, the photocurrent of hydrogen-treated TONTs (H:TONTs) significantly improved under full sunlight.

Experimental

Highly ordered TONTs were prepared by electrochemical anodization of Ti foil (99.9% purity, 0.25 mm thickness) in a

two-electrode configuration similar to a method reported previously.[13] Constant conditions (60 V for 1 h) and distance (~4 cm) between the working (Ti foil) and counter electrode (Pt mesh) were used for electrochemical anodization. The electrolyte consisted of 0.25 wt % NH_4F in ethylene glycol containing an extremely small amount of water, as reported previously.[14] All chemicals were of analytical grade. The as-anodic TONT was washed in deionized water for 5 min to remove the grown TONTs and resulted in easily peeling off the Ti substrate. As a result, the Ti substrate showing a hexagonal shaped morphology appeared and played a role as a mask during the second electrochemical anodization. The anodic reaction was again performed on this substrate in the same fresh electrolyte at 60 V for 30 min. The as-anodic TONT was washed in ethanol for 5 min, dried under nitrogen gas, and transferred to a box furnace to anneal the as-grown samples at 450 °C for 3 h under ambient air to improve the crystalline properties, followed by annealing in a mixture of H_2 and N_2 (4% of H_2) for an additional 30 min at various temperature of 350-550 ºC so the TONTs were sustainable without any destruction of intrinsic structure. As annealing temperature was increased, the color of TONTs turns from bluish to yellowish, indirectly indicating that visible light absorption resulted from narrowing of the electronic band gap of the TONTs.

Photocurrents of H:TONT electrodes were measured with a potentiostat (Autolab, 128N) using an Ag/AgCl reference electrode and a Pt mesh counter electrode. A 150 W Xe lamp (100 mW/cm^2, AM 1.5 filter) as a light source and 1 M KOH solution (pH 13.5) after nitrogen bubbling to remove the dissolved oxygen gas were employed to evaluate PEC behavior. The crystalline properties and the average grain sizes of the films were examined using high-power X-ray diffraction (HP-XRD, XPert PRO Multi Purpose X-Ray Diffractometer) with Cu K_α radiation operating at 60 kV and 55 mA. The surface morphology and thickness of the TONTs were examined by field emission scanning electron microscopy (FE-SEM, JSM-7500F, JEOL Inc., Tokyo, Japan) operating at 15 kV. Absorption spectra were obtained using Al metal and a Perkin Elmer Lambda model 900 UV-VIS-NIR absorption spectrophotometer at wavelengths of 350-600 nm. Moreover, the chemical bonding states of each element in the H:TONT were examined by X-ray photoemission spectroscopy (XPS) (PHI 5200 mode) using an Al K_α X-ray source with a chamber base pressure of ~10^{-10} Torr. Mott-Schottky plots (AUTOLAB/PGSTAT 128N, Nova) were obtained in a three-electrode cell using TONT or H:TONTs, a platinum wire, and a saturated Ag/AgCl as the working, counter and reference electrodes, respectively, to determine the flat band potential (V_{FB}) and donor concentration of the semiconducting TONT and H:TONT films. The electrolyte containing 1 M KOH solution (pH 13.5) was used, and nitrogen bubbling was carried out before taking the measurements. The electrochemical impedance spectra were obtained by applying a sinusoidal perturbation of ± 10 mV at a frequency of 1 kHz and a cell voltage of 0 V using a Nova impedance analyzer controlled by a PC.

Results and Discussion

Structural Characterization. Shown in Figure 1(a)-(c) are the top-view and cross-sectional FE-SEM images of (a) TONTs and (b, c) H:TONT films. Figure 1(a) represents a typical TONT with a length of approximately 13.5 μm grown in two-step mode.[15,16] It was noticeable that the masking layer on the surface region was deposited because there was a strong connection with the growth sequence of the anodic TONTs.[17] That is, as soon as tube growth began, a compact oxide layer was formed, followed by penetration of this layer by chemical etching of F^- ions, resulting in the formation of ordered tubes. Then, the chemical environment of electrochemical anodization affected removal of the initiation layer. In this case, the top layer remained in this electrolyte. However, H_2 treatment (550 ºC) has a profound effect on the visual appearance and morphology of the TONTs (Figure 1(b)), revealing the formation of a larger pore size and coalescence of the masking layer toward the underneath layer in comparison with that of TONTs, which was attributable to the sintering process. This may have lead to the lattice construction as a result of hydrogen incorporation, as oxygen vacancies were progressively formed. This can also increase the effect of *n*-type doping in the film. But, no discrepancy in the cross-sectional image was found in accordance with the H_2 treatment (Figure 1(c)), showing the entirely smooth walls along the vertical direction without any ripples. XRD patterns were collected from the pristine TONTs and H:TONTs prepared at various annealing temperatures to check the crystalline properties after H_2 treatment (Figure 1(d)). The observed peaks in the scanned 2θ were assigned to pure anatase phases which were consistent with the literature.[18] Additionally, it appeared that variations in the appearance of the peaks did not correspond with intensity, yet the slight shift in the (101) plane toward a longer angle was observed in the magnified view of the (101) plane. This could be explained by incorporation of hydrogen dopants in the lattice, which accelerated the creation of oxygen vacancies, and finally reduced the *d*-spacing between lattices.

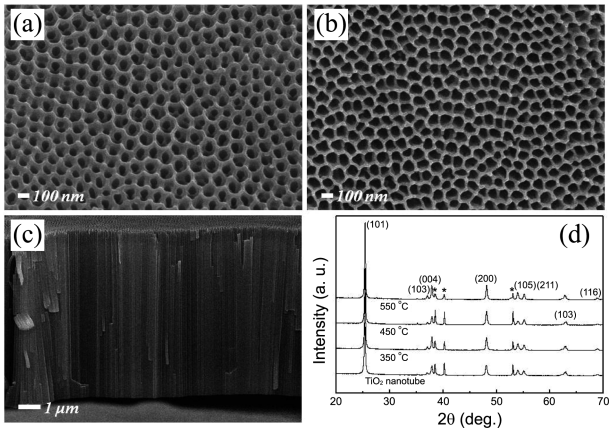

Figure 1. FE-SEM images of (a) TONT, (b) H:TONT (550 ºC), (c) the cross-sectional view of (a) and (b), and (d) XRD patterns of TONT and H:TONT film.

It was verified that the extent of the shift increased moderately with H_2 annealing temperature (not shown in here).[19]

Surface and Optical Properties. Figure 2 shows the XPS data of the Ti 2*p* and O 1*s* core level peaks to more clearly survey the variation in the chemical bonding state due to H_2 treatment of the TONT film. Light sputtering (5-6 Å) was performed before analysis to remove all surface contamination. Both films consisted of Ti (458.24 eV of Ti $2p_{3/2}$), O (529.7 eV of O 1*s*), and C (284.6 of C 1*s*), respectively. The binding energy scale was calibrated to the C 1*s* peak. In the case of TONTs film in Figure 2(a), The Ti 2*p* core level peak was designated as 485.24 eV, which was consistent with the typical value of TiO_2 containing a slightly weak shoulder on the 457 eV range indicating the partial presence of Ti^{3+} states, probably resulting from the emergence of oxygen vacancies in the intrinsic material.[20] In contrast, the Ti 2*p* core level peak of the H:TONT film (550 ºC) was shifted to a slightly lower binding energy because of the relatively abundant electrons around the Ti core metal. This was combined with a slightly asymmetric peak with a weak shoulder on the low binding energy side (approximately 457 eV) of the main peak resulting from the same TONT film. In addition, the O 1*s* core level peak of the TONT film in Figure 2(b) was 529.7 eV and containing a slightly weak shoulder on the high and low energy side attributed to the oxygen-deficient state resulting from the formation of oxygen vacancies and the formation of Ti-OH, which was located at a higher binding energy of 1.5-1.8 eV corresponding to the O 1*s* of TiO_2, respectively.[21] It is clear that H_2 treatment of the TONT film induced a modified state of chemical bonding in the Ti-O lattice and sped up the creation of oxygen vacancies, suggesting an increase in donor density of the film.

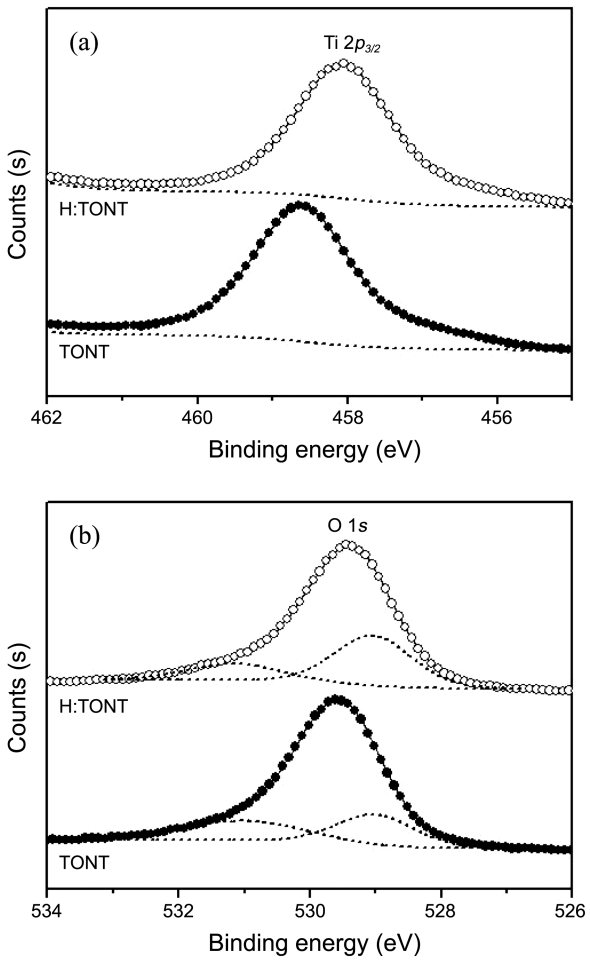

Figure 2. XPS spectra of TONT (○) and H:TONT (●, 550 ºC) film, describing the (a) Ti 2*p* and (b) O 1*s* core level peak.

Figure 3 shows the UV-vis diffuse reflectance absorption spectra of TONT and H:TONT films to verify the influence of oxygen vacancies on the optical property. Compared to the strong absorption in the UV region (< 400 nm), absorption in the visible region was relatively weak for all samples. However, the H:TONT films exhibited stronger absorbance in the visible region than that of non-treated TONT film. In particular, the extent of enhancement of the H:TONT films increased with increasing H_2 annealing temperature, probably due to the rapid creation of oxygen vacancies by hydrogen treatment, leading to a sub-band-gap transition corresponding to the excitation from the valence band to the impurity band.[22] Accordingly, the band-to-band transition from the valence band to the conduction band as well as the sub-band-gap transition concurrently happened in the H:TONT films, whereas the band-to-band transition only occurred in the pure TONT film. Thus, H_2 treatment under high temperature extended the optical absorbance toward the visible region in the TONT film, which affected PEC performance.

Electronic Properties. A Mott-Schottky plot was obtained at room temperature to investigate the variation in electronic properties caused by the H_2 treatment. According to the theory, the flat band potential (E_{FB}) and the charge carrier concentration of a semiconductor (N_d) in a specific electrochemical system can be determined by plotting the space charge capacitance, C_{sc}, of a semiconductor *versus* the applied potential (E) according to:[23]

$$1/C_{sc} = 2/(e\varepsilon_0\varepsilon N_d)(E-E_{FB})$$

where e is electronic charge (1.6×10^{-19} C), ε_0 is the permittivity of free space (8.86×10^{-12} F/m), and ε is the dielectric

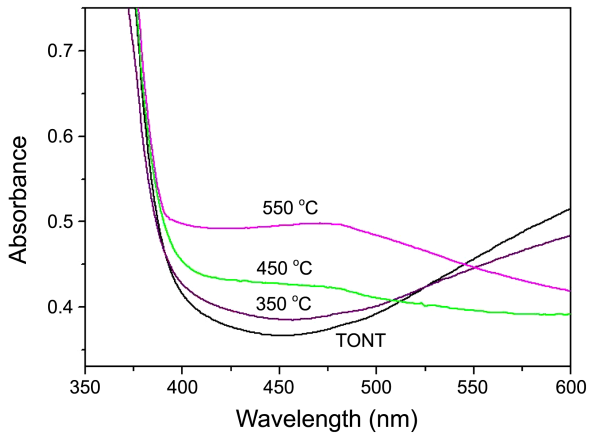

Figure 3. Absorbance spectra of TONT and H:TONT film measured under reflection mode.

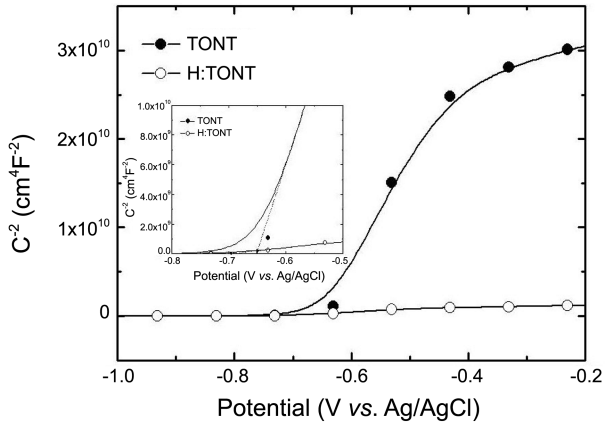

Figure 4. Mott-Schottky plots of TONT and H:TONT (550 ºC) film. (Inset: the magnified view of the Mott-Schottky plot at about −0.65 V *vs.* Ag/AgCl). Measurements were conducted at a frequency of 1 kHz with 1 M KOH solution (pH 13.5).

constant (48) of the TiO_2 material. The capacitance, C, was calculated with the following equation:

$$C = -1/2\pi fZ''$$

where f is the frequency used in the experiment and Z'' is the imaginary component of the impedance. From the above equation, we can obtain the flat band potential determined by extrapolating $C = 0$ and the charge carrier concentration from the inverse proportion of the slope if two assumptions are satisfied.[24] The first assumption is that the C is assumed to be the space charge capacitance, C_{sc}, because the space charge capacitance is 2-3 orders of magnitude smaller than the contribution of the double layer, and, thus, the contribution of the capacitance from the double layer can be neglected in the total capacitance. The second assumption is that the equivalent circuit is a series combination of a resistor and a capacitor (space charge capacitance).

Figure 4 shows the Mott-Schottky plots of the TONT and H:TONT (550 ºC) films. The E_{FB} of the TONT and H:TONT films was measured as −0.65 V and −0.7 V *vs.* saturated Ag/AgCl, respectively. The upward shift of E_{FB} in the H:TONT film was explained by the increased donor density due to hydrogen treatment, leading to improved charge separation at the semiconductor/electrolyte interface as well as favorable charge transportation.

Furthermore, the positive slope indicated that the TONT films were *n*-type semiconductors and the donor concentrations of the TONT and H:TONT films from the magnitude of the slope were 2.5×10^{17} and 9.03×10^{18} cm^{-3}, respectively, using a linear fitting method. Therefore, the H:TONT film contained 1.5 orders of magnitude higher donor concentration than that of pure TONT films due to the presence of oxygen vacancies from the H_2 treatment, which improved electrical conductivity of the TONT films.

Evaluation of PEC Performance. Figure 5(a) shows the current-voltage characteristics for the TONT and H:TONT films in the dark (dotted line) and under illumination (solid line). Compared with pure TONT film, a negative shift was

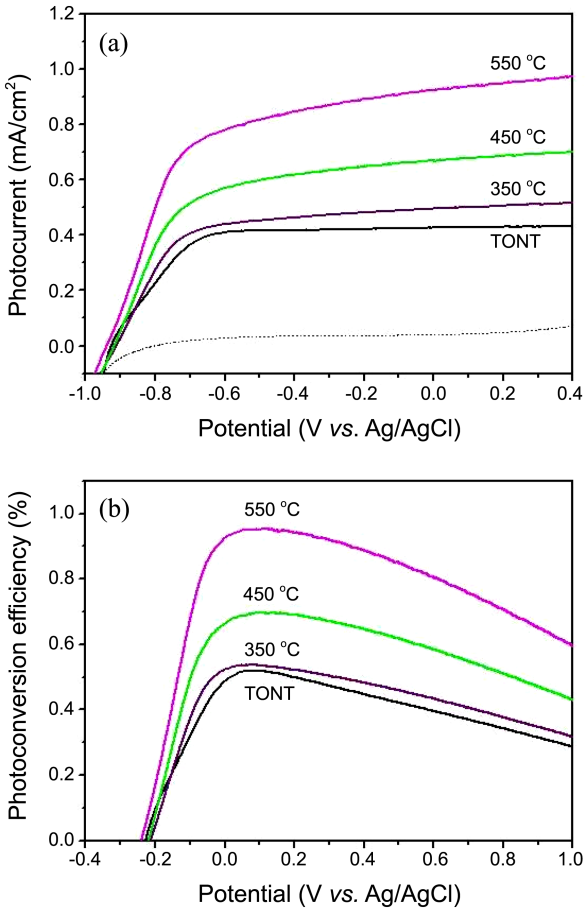

Figure 5. (a) Photocurrent response and (b) the photoconversion efficiency (%) of TONT and H:TONT film in 1 M KOH solution.

observed in the onset potential, E_{on}, from −1.0 V to −0.9 V (*vs.* NHE), similar to the upshift of the flat band potential in the Mott-Schottky plot. This was also elucidated by the formation of sub-band-gap states after H_2 treatment, which shifted E_{on} toward the negative potential. Additionally, the photocurrent densities of the H:TONT film increased gradually with the increase in H_2 annealing temperature from 350 to 550 ºC. The H:TONT film prepared at 550 ºC yielded a maximum photocurrent density of 0.967 mA/cm^2 at 0.32 V *vs.* NHE compared to 0.43 mA/cm^2 for the pure TONT film. We conclude that the photocurrent density of H:TONT (550 ºC) film were at least two times higher than that of pure TONT films in the entire potential scanned windows, demonstrating that H_2 treatment is a simple and effective method to improve PEC performance. Based on this result, the STH efficiency (η) of the TONT and H:TONT films was calculated using the following equation:[25]

$$\eta = I(1.23-V)/J_{light}$$

where V is the applied potential *versus* NHE, I is the photocurrent density at the measured potential, and J_{light} is the illumination intensity of 100 mW/cm^2 (AM 1.5G). Figure 5(b) shows the STH efficiency as a function of the applied potential. The pure TONT films exhibited maximum conversion efficiency of 0.52% at −0.61 V *vs.* NHE, whereas the

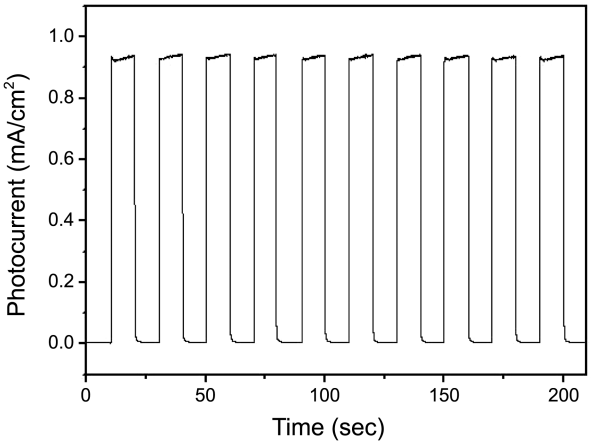

Figure 6. Photocurrent response of H:TONTs (550 ºC) films at 0 V under illumination.

H:TONT films exhibited an optimal conversion efficiency of 0.54%, 0.69%, and 0.95% in 350 ºC-treated, 450 ºC-treated, and 550 ºC-treated samples respectively, at −0.65 V *vs.* NHE, This results indicates that sequential enhancement increased with increasing annealing temperature. Thus, the hydrogen treatment substantially increased photoconversion efficiency of the TONT film by improving the maximum photocurrent density corresponding to the negative shift of the current saturation potential and reflecting favorable charge separation and transportation in the H:TONT film. These results are similar to the previous paper[25] where rutile TiO_2 nanowires were hydrogen treated, except for the optimum performance at the different annealing temperature and morphological modification after hydrogen treatment. However, the effect of hydrogen treatment is somewhat weak, relative to that of rutile TiO_2 nanowires, attributable to the different morphological properties such as wall thickness and length, different crystalline phase and substrate etc. A time-dependent measurement was performed with the H: TONT (550 ºC) film to evaluate the chemical and structural stability during PEC water splitting. The results revealed a highly stable photocurrent density of 0.93 mA/cm^2 at 0 V and repeated on/off cycles correlated with simulated solar light. In addition, no remarkable structural degradation or decrease in photocurrent was found, suggesting stable long-term solar conversion efficiency of the H:TONT film.

Conclusion

A two-step TONT film was prepared by electrochemical anodization in an electrolyte of 0.25 wt % NH_4F in ethylene glycol containing an extremely small amount of water. High-temperature annealing process under air atmosphere turned the crystalline property of the TONT film to the anatase phase. Hydrogen treatment of the film using a mixture of H_2 and N_2 gas (4% H_2) modified the electronic properties according to the annealing temperature. The structural, chemical, optical, and electronic properties of the film changed as annealing temperature was increased from 350 to 550 ºC. The H_2 treatment had a marked effect on the surface view of the TONTs, revealing the formation of larger pore diameter and coalescence of the top masking layer with the bottom layer due to the sintering process. The XPS analysis revealed that the Ti 2*p* core level peak of the H:TONT film was shifted to low binding energy sites resulting from the creation of oxygen vacancies. Furthermore, the improved light absorption in the visible wavelength range was attributable to the sub-band-gap transition from the valence band to the impurity band. Finally, the charge carrier concentration of the TONT and H:TONT films was compared using a Mott-Schottky plot, and it was confirmed that the H:TONT films contained about 1.5 orders of magnitude higher donor concentration compared to that of pure TONT films. Based on these results, the PEC performance of the TONT and H:TONT films was evaluated in a 1 M KOH solution. Approximately two times higher photocurrent density of 0.967 mA/cm^2 at 0.32 V *vs.* NHE was achieved in the H:TONT film (550 ºC) relative to 0.43 mA/cm^2 for the pure TONT film. Furthermore, the η of the H:TONT films were 0.95%, whereas a 0.52% STH efficiency was obtained for the TONT films. In addition, the stable long-term solar conversion efficiency of the H:TONT films was confirmed by repeated on/off cycles using simulated solar light and was not accompanied by structural degradation or a decrease in photocurrent. Therefore, it can be concluded that hydrogen treatment of TONT films would overcomes the intrinsic material properties to enhance PEC performance.

Acknowledgments. This study was supported by the National Research Foundation of Korea Grant funded by the Korean Government (Ministry of Education, Science and Technology). (2011-0013154) (SHK). This study was also financially supported by Chonnam National University, 2011.

References

1. Fujishima, A.; Honda, K. *Nature* **1972**, *238*, 37.
2. Ni, M.; Leung, M. K. H.; Leung, D. Y. C.; Sumathy, K. *Renewable Sustainable Energ. Rev.* **2007**, *11*, 401.
3. Walter, M. G.; Warren, E. L.; McKone, J. R.; Boettcher, S. W.; Mi, Q. X.; Santori, E. A.; Lewis, N. S. *Chem. Rev.* **2010**, *110*, 6446.
4. Mohapatra, S. K.; Misra, M.; Mahajan, V. K.; Raja, K. S. *J. Catal.* **2007**, *246*, 362.
5. Liu, M.; Snapp, N.; Park, H. *Chem. Sci.* **2011**, *2*, 80.
6. Hwang, Y. J.; Hahn, C.; Liu, B.; Yang, P. *ACS Nano* **2012**, *6*, 5060.
7. Mor, G. K.; Prakasam, H. E.; Varghese, O. K.; Shankar, K.; Grimes, C. A. *Nano Lett.* **2007**, *7*, 2356.
8. Linsebigler, A. L.; Lu, G.; Yates, J. T. *Chem. Rev.* **1995**, *95*, 735.
9. Shi, J.; Hara, Y.; Sun, C.; Anderson, M. A.; Wang, X. *Nano Lett.* **2011**, *11*, 3413.
10. Ma, X.; Wu, Y.; Lu, Y, Xu, J.; Wang, Y.; Zhu, Y. *J. Phys. Chem. C* **2011**, *115*, 16963.
11. Nakamura, R.; Tanaka, T.; Nakato, Y. *J. Phys. Chem. B* **2004**, *108*, 10617.
12. Sang, L.; Zhi-yu, Z.; Guang-mei, B.; Chun-xu, D.; Chong-fang, M. *Int. J. Hydrogen Energy* **2012**, *37*, 854.
13. Kang, S. H.; Kim, J.-Y.; Kim, H. S.; Sung, Y.-E. *J. Ind. Eng. Chem.* **2008**, *14*, 52.
14. Prakasam, H. E.; Shankar, K.; Paulose, M.; Varghese, O. K.;

Grimes, C. A. *J. Phys. Chem. C* **2007**, *111*, 7235.
15. Kang, C.; Xie, Y.; Xie, E. *Optoelectron. Adv. Mater.-Rapid Commun*. **2011**, *5*, 518.
16. Ji, Y.; Lin, K.-C.; Zheng, H.; Zhu, J.-J.; Samia, A. C. S. *Electrochem. Comm*. **2011**, *13*, 1013.
17. Mir, N.; Lee, K.; Paramasivam, I.; Schmuki, P. *Chem. Eur. J.* **2012**, *18*, 11862.
18. Kang, S. H.; Lim, J.-W.; Kim, H. S.; Kim, J.-Y.; Sung, Y.-E. *Chem. Mater.* **2009**, *21*, 2777.
19. Chae, Y.; Park. J.; Mori, S.; Suzuki, M. J. *Ind. Eng. Chem.* **2012**, *18*, 1572.
20. Kang, S. H.; Kim, J.-Y.; Sung, Y.-E. *J. Phys. Chem. C* **2007**, *111*, 9614.
21. Lazarus, M. S.; Sham, T. K. *Chem. Phys. Lett*. **1982**, *92*, 670.
22. Gao, H.; Dai, Z. D.; Qu, Y. *Chem. Eng. Technol*. **2009**, *32*, 867.
23. Barsoukov, E.; Macdonald, J. R. *Impedance Spectroscopy Theory, Experiment, and Applications*; Wiley: New Jersey, 2005; chapter 4.
24. Fabregat-Santiago, F.; Garcia-Belmonte, G.; Bisquert, J.; Bogdanoff, P.; Zaban, A. *J. Electrochem. Soc*. **2003**, *150*, E293.
25. Wang, G.; Wang, H.; Ling, Y.; Tang, Y.; Yang, X.; Fitzmorris, R. C.; Wang, C.; Zhang, J. Z.; Li, Y. *Nano Lett.* **2011**, *11*, 3026.